Talanta 226 (2021) 122099

Contents lists available at ScienceDirect

Talanta

journal homepage: www.elsevier.com/locate/talanta

Response surface methodology optimized electrochemical DNA biosensor based on HAPNPTs/PPY/MWCNTs nanocomposite for detecting *Mycobacterium tuberculosis*

Kobra Salimiyan Rizi [a,1], Behnaz Hatamluyi [b,c,1], Majid Rezayi [b,d,*], Zahra Meshkat [a], Mojtaba Sankian [e], Kiarash Ghazvini [a], Hadi Farsiani [a], Ehsan Aryan [a,**]

[a] Antimicrobial Resistance Research Center, Department of Medical Bacteriology and Virology, Qaem University Hospital, School of Medicine, Mashhad University of Medical Sciences, Mashhad, Iran
[b] Medical Toxicology Research Center, Mashhad University of Medical Sciences, Mashhad, Iran
[c] Student Research Committee, Mashhad University of Medical Sciences, Mashhad, Iran
[d] Department of Medical Biotechnology and Nanotechnology, School of Medicine, Mashhad University of Medical Sciences, Mashhad, Iran
[e] Division of Immunobiochemistry, Immunology Research Centre, Bu- Ali Research Institute, Mashhad University of Medical Sciences, Mashhad, Iran

ARTICLE INFO

Keywords:
Electrochemical DNA biosensor
Response surface methodology
Mycobacterium tuberculosis diagnosis
Polypyrrole
Hydroxyapatite nanoparticles

ABSTRACT

An important issue in the prognosis of tuberculosis (TB) is a short period between correct diagnosis and start the suitable antibiotic therapy. So, a rapid and valid method for detection of *Mycobacterium tuberculosis* (*M. tb*) complex is considered as a necessity. Herein, a rapid, low-cost, and PCR-free DNA biosensor was developed based on multi-walled carbon nanotubes (MWCNTs), polypyrrole (PPy), and hydroxyapatite nanoparticles (HAPNPs) for highly sensitive and specific recognition of *M.tb*. The biosensor consisted of *M.tb* ssDNA probe covalently attached to the HANPs/PPy/MWCNTs/GCE surface that hybridized to a complementary target sequence to form a duplex DNA. The *M.tb* target recognition was based on the oxidation signal of the electroactive Methylene Blue (MB) on the surface of the modified GCE using differential pulse voltammetry (DPV) method. It is worth to mention that for the first time Plackett-Burman (PB) screening design and response surface method (RSM) based on central composite design (CCD) was applied as a powerful and an efficient approach to find optimal conditions for maximum *M.tb* biosensor performance leading to simplicity and rapidity of operation. The proposed DNA biosensor exhibits a wide detection range from 0.25 to 200.0 nM with a low detection limit of 0.141 nM. The performance of designed biosensor for clinical diagnosis and practical applications was revealed through hybridization between DNA probe-modified GCE and extracted DNA from sputum clinical samples.

1. Introduction

Mycobacterium tuberculosis, the causative agent of tuberculosis (TB), is a member of the specie *Mycobacterium tuberculosis* complex [1]. Despite recent medical advances, TB is still one of the top 10 causes of death in the world, so it has become a public health concern worldwide [2,3]. Following inhalation of the aerosol droplets include tubercle bacilli, if the human innate immune defenses failure to eliminate the bacteria, M. tb start to replicating inside alveolar macrophages and at the next step, it spreads to other tissues and organs via the bloodstream and lymphatic [4]. Today, control of the universal burden of TB is blocked due to a lack of simple, valid, rapid, and cost-effective diagnostic methods that can be used in resource poor-settings [5]. A lot of research studies have been done in this area over the last few decades to evolve beneficial point of care diagnostic methods that are cheap, robust and can be done at high throughput in rural regions [6]. The conventional methods such as culture testing [7], sputum smear microscopy [8] and chest X-radiography [9] are not usable for immunocompromised persons or even have not enough speed for analysis, sensitivity, discriminatory power, and specificity [10,11]. Nowadays, biosensors have attracted significant attention for their friendly usage, availability, miniaturization, continuous monitoring, and real-time results [12].

* Corresponding author. Medical Toxicology Research, Center, Mashhad University of Medical Sciences, Mashhad, Iran.
** Corresponding author.
E-mail addresses: rezaeimj@mums.ac.ir (M. Rezayi), aryane@mums.ac.ir (E. Aryan).
[1] Equal as a first author.

https://doi.org/10.1016/j.talanta.2021.122099
Received 15 September 2020; Received in revised form 26 December 2020; Accepted 5 January 2021
Available online 11 January 2021
0039-9140/© 2021 Elsevier B.V. All rights reserved.

Table 1
Oligonucleotide sequences employed.

Oligonucleotide name	Length	Sequence
Probe DNA (p IS6110)	21	5′- CAAAGTGTGGCTAACCCTGAA-3′
Complementary Target DNA(t IS6110)	21	5′- TTCAGGGTTAGCCACACTTTG-3′
2 Mismatch target DNA-1	21	5′- TTCGGGGGTAGCCACACTTTG-3′
5 Mismatch target DNA-2	21	5′- TTCGGGGGTTGCCTCACTATG -3′
Non-Complementary Target DNA (t IS6110)	21	5′- AAGCACTGATTGGCATAGAAC-3′

Among them, the development of DNA biosensors or genosensors based on the hybridization between DNA targets and complementary probes have been increased in recent years [13]. They can have the potential for point-of-care infectious detections in societies with a high burden of tuberculosis and with the limitation to access reference laboratories [14,15]. The sensitivity of electrochemical sensors and biosensors is affected by the characteristics of the electrode surface modifier [16–18]. So far, a variety of nanomaterial has been developed and used to improve sensitivity by enhancing the conductivity, surface area of the electrode, and to form an ideal immobilization material for biomolecules [19]. Therefore, we used multi-walled carbon nanotubes (MWCNTs) due to its great electrical conductivity, high surface-to-volume ratio, and chemical inertness [20]. Moreover, the use of organic polymers such as polypyrrole (PPY) in biosensor fabrication increases biocompatibility, conductivity, chemical stability, and reduces toxicity [21–23]. Reliable immobilization of biomolecules on the electrode surface is an important step in fabricating biosensors. Hydroxyapatite nanoparticles (HAPNPs) as an essential biomaterial are used as immobilizing substrates for biomolecules [24–26]. The good bioactivity, great biocompatibility, non-toxic, and particular multi-adsorbing sites are all favorable features that allow HAPNPs to be used in biosensors [27,28]. However, identifying and optimizing the significant factors and achieving a competent result with fewer trials is a major challenge in constructing biosensors. Therefore, the development of multivariate techniques is particularly important for the optimization of different operating conditions. Response surface method (RSM) is defined as an assemblage of statistical techniques for experimental design, evaluating the main effective factors, searching optimum conditions, creating a suitable model, and predicting the responses at optimized conditions. The usual practice, which a parameter changes at one time cannot investigate the combined effects of all factors and requires a significant amount of tests, chemicals, and time [29]. For overcoming these limitations, RSM as a practical designing program can be employed to detect various interactions among different parameters and obtaining the best optimum conditions for a multivariable system [30]. In this work, we present a novel DNA biosensor system for sensitive and selective detection of specific nucleic acid sequence characteristic for *M. tb*. Based on the excellent synergistic effects between HAPNPs, PPY, and MWCNTs as well as specific hybridization between DNA probe-modified GCE and extracted DNA from clinical sputum samples, a simple, low cost, and potent biosensor was introduced.

2. Experimental details

2.1. Reagents

MWCNTs (purity ˃95%) were prepared from DropSens (Asturias, Spain) with average diameter of 10 nm and the average length of 1–2 μm. Pyrrole, N,N-dimethylformamide (DMF), Potassium ferricyanide [$K_3Fe(CN)_6$], sodium hydroxide (NaOH), sodium chloride (NaCl), Methylene blue (MB), sodium hydrogen phosphate (Na_2HPO_4), sodium dihydrogen phosphate (NaH_2PO_4), nitric acid (HNO_3), and sulfuric acid (H_2SO_4) were of analytical grade and purchased from Merck. Hydroxyapatite nanoparticles (HAPNPs) were synthesized based on sol-gel method reported in our previous study [31]. Synthetic single-stranded DNA (ssDNA) oligonucleotides, purified with high performance liquid chromatography (HPLC), were purchased from Macrogen Company (South Korea). The oligonucleotide sequences used are given in Table 1.

2.2. Apparatus

The voltammetry measurements were performed using a potential state (Autolab-PGSTAT204, Metrohm, Netherlands) equipped with a three-electrode system which was configured by connecting a glassy carbon electrode, GCE (i.d. = 3.0 mm) modified with MWCNTs, PPY,

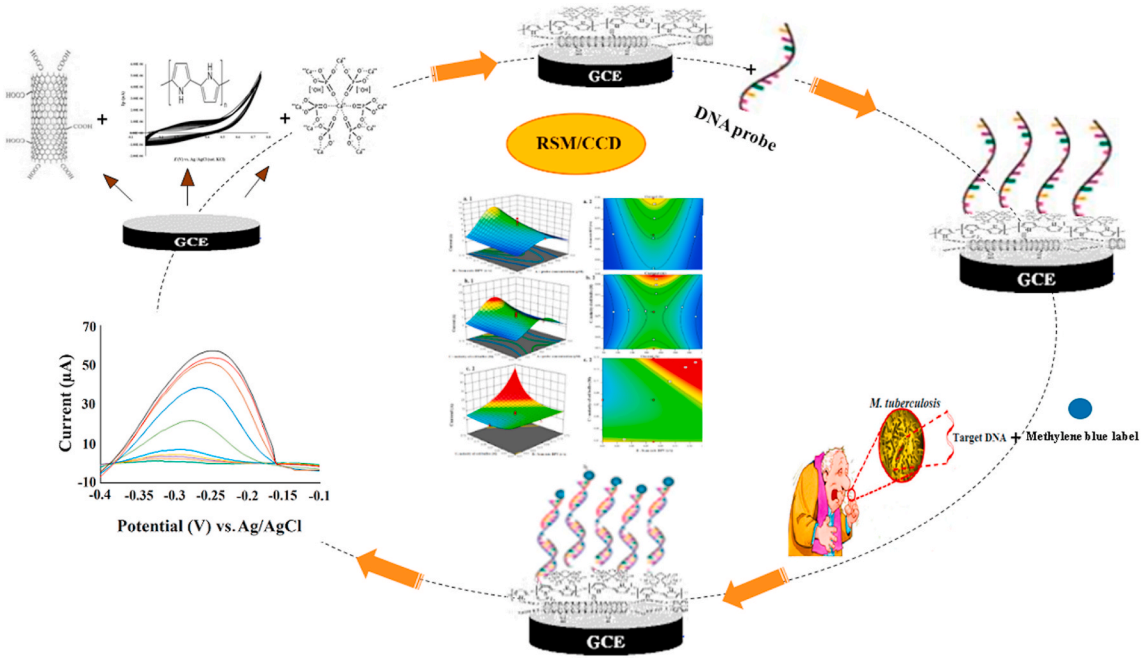

Scheme 1. Schematic representation of the electrochemical DNA biosensor.

HAPNPs, and ssDNA (ssDNA/HAPNPs/PPY/MWCNTs) as working electrode, a platinum wire as auxiliary electrode, and an Ag/AgCl electrode as a reference electrode. Other equipment used to characterize the electrode surface was: field emission scanning electron microscopy (FE-SEM) (TESCAN MIRA3-FEG) and atomic force microscopy (AFM) PK NanoWizard (JPK, Germany).

2.3. Bioinformatics' experiments

The insertion element IS6110 sequence was chosen for detecting MTBC. The probe strand spans bases 611–632 within the insertion sequence (IS) 6110 of *M. tuberculosis* H37Rv (Accession No: NC_000662.2) that was used as for bioinformatics process. Bio Edit sequence alignment editor 7.2.5 software (Hall 1999) with the aid of ClustalW algorithm as applied for alignment of selected nucleotide sequences [32–34].

2.4. M. tb DNA biosensor preparation

2.4.1. Fabrication of HAPNPs/PPY/MWCNTs/GCE

The HAPNPs/PPY/MWCNTs/GCE was fabricated via the following three step procedure: in first step, acid treatment of MWCNTs to produce carboxylic acid-functionalized MWCNTs (MWCNTs–COOH) was done according to the previously reported procedure [35]. A bare glassy carbon electrode was mechanically polished with 0.3 μm alumina slurry, followed by rinsing with distilled water and next bath sonication in ethanol: water (50:50, v/v) solution for 3 min. Subsequent rinsed with double distilled water. The MWCNT suspension was produced by dissolving 0.1 mg of MWCNTs-COOH in 2 mL of DMF and ultra-sonicated for 30 min so that giving a black dispersion. The MWCNTs/GCE was fabricated by drop casting of 10 μL MWCNTs suspension on the GCE and left to dry in oven at 45 °C for 10 min. In second step, the MWCNTs/GCE was immersed in a solution containing 0.5 M pyrrole prepared in phosphate buffered solution (PBS, pH = 7.4, 0.1M) and cyclic voltammetry (CV) was done in potential range between −0.2 and + 0.8 V at a scan rate of 50 mV s^{-1} for a total of 15 cycles. This process gave PPY/MWCNTs/GCE. Finally, in the third step, 10 μl of a 500 μg mL^{-1} HAPNPs (dispersed in PBS, pH = 6.5, 0.05M) was coated on PPY/MWCNTs/GCE and dried at ambient temperature to obtain the HAPNPs/PPY/MWCNTs/GCE.

2.4.2. DNA probe immobilization

To immobilize the ssDNA probe on the electrode surface, the HAPNPs/PPY/MWCNTs/GCE was immersed in 150 μL of 250 pM ssDNA probe in PBS, (pH 7.0, 0.05 M) for 1 h at ambient temperature. Subsequently, to remove any unbounded ssDNA probe, the electrode was washed with ultrapure water and used for detection. A possible covalent bonding could happen among the phosphate group of DNA with negative electric charge and calcium groups of HAPNPs with positive surface charge [36,37]. The schematic representation of the fabrication and detection process of the *M.tb* biosensor is displayed in Scheme 1.

2.5. Hybridization and electrochemical measurements

For hybridization, the probe-modified electrode was incubated into PBS (pH 7.0, 0.05 M) containing different concentrations of target DNA and methylene blue (MB, 500 μM) for 20 min at 59.4 °C. Afterwards, the electrode was washed with PBS to remove non-bounded DNA. In this study, MB was used as electrochemical indicator. MB can be attached to the negative-charged phosphate group of dsDNA through electrostatic interaction [38,39]. By increasing target DNA concentration and formation of dsDNA, the accumulation of MB in the dsDNA groove increased, consequently the oxidation peak current of the MB also enhanced. Therefore, the peak current of MB was considered as analytical signal. For the detection studies, the differential pulse voltammetry (DPV) measurements were carried out in the potential range from −0.4 to −0.1 V with modulation time of 0.020 s, potential step of 5 mV, time interval of 0.0329 s, and amplitude of modulation of 25 mV. All electrochemical measurements were repeated three times.

Table 2
The experimental field definition for PB.

Variable	Symbol	Low(−)	High(+)
Probe concentration (pM)	A	50	750
Probe immobilization time (min)	B	30	90
Scan rate of polypyrrole electrodeposition (V/s)	C	0.01	0.1
Scan rate of DPV(V/s)	D	0.01	0.15
Molarity of cell buffer (M)	E	0.01	0.15
pH of cell buffer	F	6.0	7.5
Temperature of hybridization (°C)	G	25	65
Time of hybridization (min)	H	25	65
Molarity of hybridization buffer (M)	J	0.01	0.15
pH of hybridization buffer	K	6.0	7.5
Temperature of probe immobilization (°C)	L	25	60

2.6. Statistical treatment of data

In the present study, experimental design, statistical analyses, the response surface modeling, and 3D response surface plots to achieve the optimum conditions were done utilizing the Design Expert 7.0.0- trial (Stat-Ease Inc., Minneapolis, USA).

3. Results and discussions

3.1. Optimization of analytical conditions

In the manufacture of electrochemical biosensors, the use of multivariate optimization methods leads to faster, more efficient and economical access to optimal conditions [40,41]. Accordingly, in the first step of DNA biosensor optimization, a Plackett–Burman (PB) experimental design was applied to identify the main factors affecting on the analytical response. For this purpose, eleven factors including probe concentration (A), probe immobilization time (B), scan rate of electrodeposition of PPY (C), scan rate of DPV measurements (D), molarity of cell buffer (E), pH of cell buffer (F), temperature of hybridization (G), time of hybridization (H), molarity of hybridization buffer (J), pH of hybridization buffer (K), and temperature of probe immobilization (L) were screened by conducting 12 experiments at two levels, high level (+) and a low level (−). Table 2 presented the factors, symbols as well as low and high levels, and Table 3, presented the PB experimental design matrix for the mentioned variables together with the analytical response for each run.

The screening process of these eleven factors and statistical evaluation of results at a 95% confidence level ($p \leq 0.05$) presented the Pareto chart as displayed in Fig. 1. Based on the Lenth approach [41] between the variables screened, the most influencing factors for DNA biosensor fabrication were in the order of molarity of cell buffer (E), probe concentration (A), and DPV scan rate (D). It was also found that the effect of other factors on the electrode response was not statistically significant. Therefore, their optimal level was obtained based on our preliminary experiments using the one-factor-at-a-time (OFAT) method.

In the second step, a set of 20 tests were designed using the central composite design (CCD) to find the optimal values, interaction, and main effect of statistically significant factors including molarity of cell buffer, probe concentration, and DPV scan rate on the DNA biosensor response, as shown in Table 4.

The relationship between the DNA biosensor response (peak current) and process parameters were approximated by the following quadratic equation (Eq. (1)):

$$Current(\mu A) = +1.82 + 0.0801A + 0.5223D + 0.1905E - 1.70A\hat{2} + 0.6340E\hat{2} + 0.6017DE \quad (1)$$

Table 3
PB experimental design matrix for eleven variables.

Exp. no	Variables											
Run	A	B	C	D	E	F	G	H	J	K	L	Current (μA)
1	50	30	0.01	0.025	0.01	6	25	25	0.01	6	25	17.10
2	750	30	0.01	0.025	0.15	6	65	65	0.01	7.5	60	86.80
3	50	90	0.1	0.025	0.15	7.5	65	25	0.01	6	60	132.73
4	50	90	0.1	0.2	0.01	6	25	65	0.01	7.5	60	17.80
5	750	90	0.01	0.2	0.15	7.5	25	25	0.01	7.5	25	80.00
6	50	30	0.1	0.025	0.15	7.5	25	65	0.15	7.5	25	129.8
7	750	90	0.01	0.025	0.01	7.5	25	65	0.15	6	60	24.00
8	50	30	0.01	0.2	0.01	7.5	65	25	0.15	7.5	60	13.80
9	750	30	0.1	0.2	0.15	6	25	25	0.15	6	60	76.00
10	50	90	0.01	0.2	0.15	6	65	65	0.15	6	25	117.10
11	750	90	0.1	0.025	0.01	6	65	25	0.15	7.5	25	21.48
12	750	30	0.1	0.2	0.01	7.5	65	65	0.01	6	25	16.40

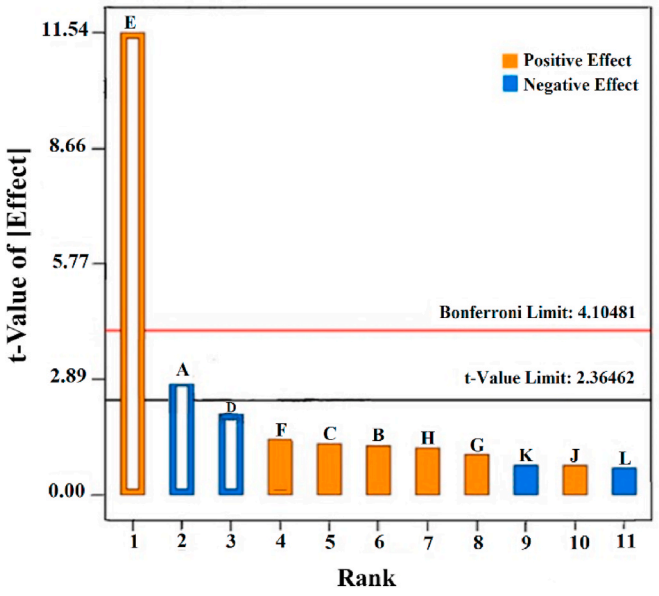

Fig. 1. The standardized main effect Pareto chart for PB.

Table 4
Experimental plan for optimization of DNA biosensor using CCD.

Exp. no	E; molarity of cell buffer (M)	A; probe concentration (pM)	D; DPV scan rate (V/s)	Current (μA)	
				Predicted	Actual
1	0.08	400	0.08	6.83	8.8
2	0.08	400	0.15	8.1	8.3
3	0.08	400	0.08	6.83	7.8
4	0.01	400	0.08	9.1	7.9
5	0.15	50	0.15	7.5	6.5
6	0.08	400	0.08	6.83	6.4
7	0.15	750	0.15	11.1	11.3
8	0.15	750	0.01	1.95	1.0
9	0.01	50	0.15	1.1	2.0
10	0.01	750	0.01	1.2	2.1
11	0.08	400	0.01	4.05	4.0
12	0.15	50	0.01	0.4	0.7
13	0.08	400	0.08	6.829	7.3
14	0.15	400	0.08	12.65	14
15	0.01	50	0.01	2.175	1.9
16	0.01	750	0.15	2.1	1.7
17	0.08	400	0.08	6.83	5.5
18	0.08	50	0.08	0.81	1.0
19	0.08	750	0.08	6.829	4.8
20	0.08	400	0.08	6.83	8.8

Where A, D, and E are probe concentration, scan rate of DPV, and molarity of cell buffer, respectively. The analysis of the variance (ANOVA) was applied to evaluate the sufficiency of the developed regression model (Table 5). The amount of F-value (28.94) and low p-value (<0.0001) implies the model is significant. Goodness-of-fit for the proposed model was confirmed by the coefficient of determination (R^2 = 0.9666 and adjusted R^2 = 0.9332). The P-value of lack of fit (LOF) was 0.4309 indicating LOF was not significant and the model was well adapted to the response.

The perturbation plot in Fig. S1 revealed that the molarity of cell buffer (factor C) had the most significant influence on the current response and the influence of other two factors (probe concentration and DPV scan rate) was less significant when compared to the molarity of cell buffer. It also revealed that probe concentration has a Gaussian effect on biosensor response. Primarily, by increasing of probe concentration (factor A) up to 400 pM the DPV response increased. In the concentration range of 400–750, the DPV response leveled off. It can be described by the lower availability of the methylene blue (a basic dye of thiazine series) and massive probe accumulation on the surface of GCE that induces probe overloading [42–45]. Loaiza et al., was reported that oxidation signal decreases probably due to the blocking effect of the working electrode surface by the excess amount of immobilized DNA probe [46]. DPV scan rate (factor B) approximately had a positive linear effect on biosensor response. By increasing the DPV scan rate the biosensor response increased, too. The results also showed that by increasing the molarity of cell buffer up to 0.08 M, the DPV response decreased while it was observed an increase in response from 0.08 to 0.15 M. The interactive effects of independent variables on biosensor response was evaluated by 3D response surface and 2D contours plots as displayed in Fig. 2. With DPV peak current as of the response, the 3D response surface and 2D contours plots presented the interaction effects between DPV scan rate and probe concentration (Fig. 2A), molarity of cell buffer and probe concentration (Fig. 2B), and molarity of cell buffer and DPV scan rate (Fig. 2C).

The optimum conditions predicted by RSM model with the highest response were selected for fabrication of the DNA biosensor. The optimal variables obtained as: ssDNA probe concentration 354 pM, molarity of cell buffer 0.12 M, and DPV scan rate 0.15 V/s. Optimized parameters predicted by RSM were then verified with a series of experiments to produce the actual current response. The presented results in Table S1 show that the obtained peak current is in good agreement with the predicted value by the RSM model.

3.2. *Morphological and electrochemical characterization*

Morphological characterization was studied at each step by means of FE-SEM. Fig. 3 shows the surface morphology of bare GCE, MWCNTs/GCE, PPY/MWCNTs/GCE, and HAPNPs/PPY/MWCNTs/GCE, respectively. In Fig. 3B, FE-SEM image of MWCNTs/GCE depicted a randomly

Table 5
ANOVA analysis for quadratic equation modeling of effective parameters on DNA biosensor fabrication.

Source	Sum of Squares	df	Mean Square	F-value	p-value	
Model	14.23	9	1.58	28.94	<0.0001	significant
A-probe concentration	0.0536	1	0.0536	0.9813	0.3478	
B-scan rate DPV	2.73	1	2.73	49.93	<0.0001	
C-molarity of cell buffer	0.3627	1	0.3627	6.64	0.0299	
AB	0.0005	1	0.0005	0.0100	0.9223	
AC	0.1181	1	0.1181	2.16	0.1756	
BC	2.90	1	2.90	53.00	<0.0001	
A^2	5.11	1	5.11	93.57	<0.0001	
B^2	0.0024	1	0.0024	0.0445	0.8377	
C^2	0.9378	1	0.9378	17.16	0.0025	
Residual	0.4918	9	0.0546			
Lack of Fit	0.2354	4	0.0589	1.15	0.4309	not significant
Pure Error	0.2563	5	0.0513			
Cor Total	14.73	18				

$R^2 = 0.9666$, Adjusted $R^2 = 0.9332$, Predicted $R^2 = 0.8133$, C.V. % = 17.02, Adeq Precision = 17.675.

entangled and flattish surface morphology. After wrapping of MWCNTs/GCE surface with PPY through electropolymerization, granular like particles and disordered structure could be seen in MWCNTs surface (Fig. 3C). Comparatively to the FE-SEM micrographs of PPY/MWCNTs/GCE, the HAPNPs/PPY/MWCNTs/GCE presented several supplementary brighter nanocrystalline particles, which can be assigned to the HAPNPs (Fig. 3D).

Further, the surface properties of modified electrodes were examined with AFM. The root-mean-squared (RMS) roughness of HAPNPs/PPY/MWCNTs/GCE, ssDNA/HAPNPs/PPY/MWCNTs/GCE, and dsDNA/HAPNPs/PPY/MWCNTs/GCE were assessed and measured as 34.71 nm, 76.08 nm, and 123.2 nm, respectively. The increase in the RMS roughness of the ssDNA/HAPNPs/PPY/MWCNTs/GCE to HAPNPs/PPY/MWCNTs/GCE proved the accumulation of ssDNA probe on the surface of the electrode (Fig. 3E and F). After the hybridization process, a further increase of the RMS roughness (123.2 nm) was observed (Fig. 3G), due to the reduction of flexibility and the occurrence of the elastic deformation phenomenon [47,48].

Cyclic voltammetry (CV) technique was applied for the electrochemical characterization of different films on a surface-modified electrode in each fabrication process. In this study, the CV voltammograms for different electrodes were recorded using 1.0 mM K_3 [Fe $(CN)_6$]/K_4[Fe$(CN)_6$] solution containing 0.1 M KCl as an electrochemical probe (Fig. 4A). For bare GCE, a pair of redox peaks could be observed in Fig. 4A (curve a), while remarkable increase was accrued in anodic and cathodic peak current for MWCNTs/GCE and PPY/MWCNTs/GCE (curve b and c) indicating that MWCNTs and PPY served as an ideal conductive material increasing effective surface area and accelerating the electron transfer rate of [Fe $(CN)_6]^{3-/4-}$. After decorating HAPNPs on the PPY/MWCNTs/GCE, the CV peak currents clearly increased further (curve d) due to synergistic effects between MWCNTs, PPY and HAPNPs. These results implied that the assemble MWCNTs, PPY and HAPNPs on the GCE surface effectively improved the detection sensitivity of the constructed platform. The subsequent incubation of the modified electrode in the ssDNA probe solution caused a dramatic decrease of redox currents (curve e), because of the electrostatic repulsion between the negatively charged DNA and [Fe $(CN)_6]^{3-/4-}$. With the introduction of complementary DNA, the negative charge was increased and repulsion of redox species was enhanced [49]. Therefore, the intensities of the CV peak currents were decreased slightly (curve f). In order to assess the importance of deposited nanostructures on biosensor performance, the effective surface area of different modified electrodes was calculated using Randles-Sevcik's model [50,51] by measuring the peak current variation at various scan rates between 10 and 250 mV s^{-1}. The electroactive surface area was estimated from the slope of the peak current vs. $v^{1/2}$ plot (Fig. 4B). Accordingly, the electroactive surface areas of bare GCE, MWCNTs/GCE, PPY/MWCNTs/GCE, and HAPNPs/PPY/MWCNTs/GCE were determined to be 0.21, 0.34, 0.64, and 0.87 cm^2, respectively. The results of Randles-Sevcik's model obviously prove that developed HAPNPs/PPY/MWCNTs/GCE sensing platform capable of enhancing a greater amount of effective surface area to provide better sensitivity.

FTIR analysis was performed to characterize the modified electrode before and after the probe immobilization (Fig. 5). FTIR spectra of MWCNT/PPy/KHApNps (Fig. 5A) showed strong Ca–O stretching, and C–H stretching absorptions at around 3444 cm^{-1} and 2917.14 cm^{-1}, respectively [52,53]. The intensity that has been observed at the 3444 cm^{-1} band is due to the configuration freedom CaO groups and so the Ca atoms have more vibration at this position. The bands at 520.84 cm^{-1} and 1057.27 cm^{-1} were assigned to the molecular vibrations *v*2 and *v*3 phosphate groups PO_4^{3-} moiety, respectively [54]. The band at 1057.27 cm^{-1} shows the symmetric stretching of P–O [55]. FT-IR spectra of ssDNA/MWCNT/PPy/KHApNps electrode surface (Fig. 5B) shows the reduction some peaks at 3444 cm^{-1}, 1057 cm−1, 520.84 cm^{-1} and 453.16 cm^{-1}. The appearance of some new peaks at <1000 cm^{-1} can be correspond to the stretching of C–N and phosphates groups, respectively confirming the presence of acids nucleic on the modified electrode surface [56]. These results suggest the covalent attachment of ssDNA onto the MWCNT/PPy/KHApNps electrode surface [57,58].

3.3. Dynamic range and detection limit of the biosensor

Under the optimized experimental conditions, DPV measurements were carried out by using different concentrations of target DNA to evaluate the dynamic range and sensitivity of the developed biosensor. As depicted in Fig. 6A, the peak current of MB increased with the increase of target DNA concentration. This electrochemical response is due to the formation of the dsDNA structure on the surface of the electrode, which further increases the accumulation of MB on the electrode. As shown in Fig. 6B, a well linear relationship was obtained between the MB peak current and the logarithm of target concentration in the dynamic range from 0.25 to 200.0 nM with regression equation of $I_P = 18.201 \log C + 15.208$ ($R^2 = 0.9919$, n = 3) where I_P was the MB peak current intensity and C was the concentration of target DNA. The detection limit of this DNA biosensor was estimated to be 0.141 nM. This result was calculated when the linear regions of the calibration graphs were extrapolated to the baseline currents [59–63].

In addition, thanks to the large specific surface area and high electron transfer ability provided by the HAPNPs/PPY/MWCNTs nanocomposite, the proposed DNA biosensor presented comparable features compared to previously reported *M. tb* biosensors in the literature (Table S2). Although some biosensors have shown lower detection limits [64,65], they have a narrower linear range. In the clinic, the sputum of TB patients has been scored by the number of acid-fast bacilli per volume (David HL, CDC, 1996) so if a biosensor had a narrow dynamic range it will be saturated immediately. So, for clinical samples with a

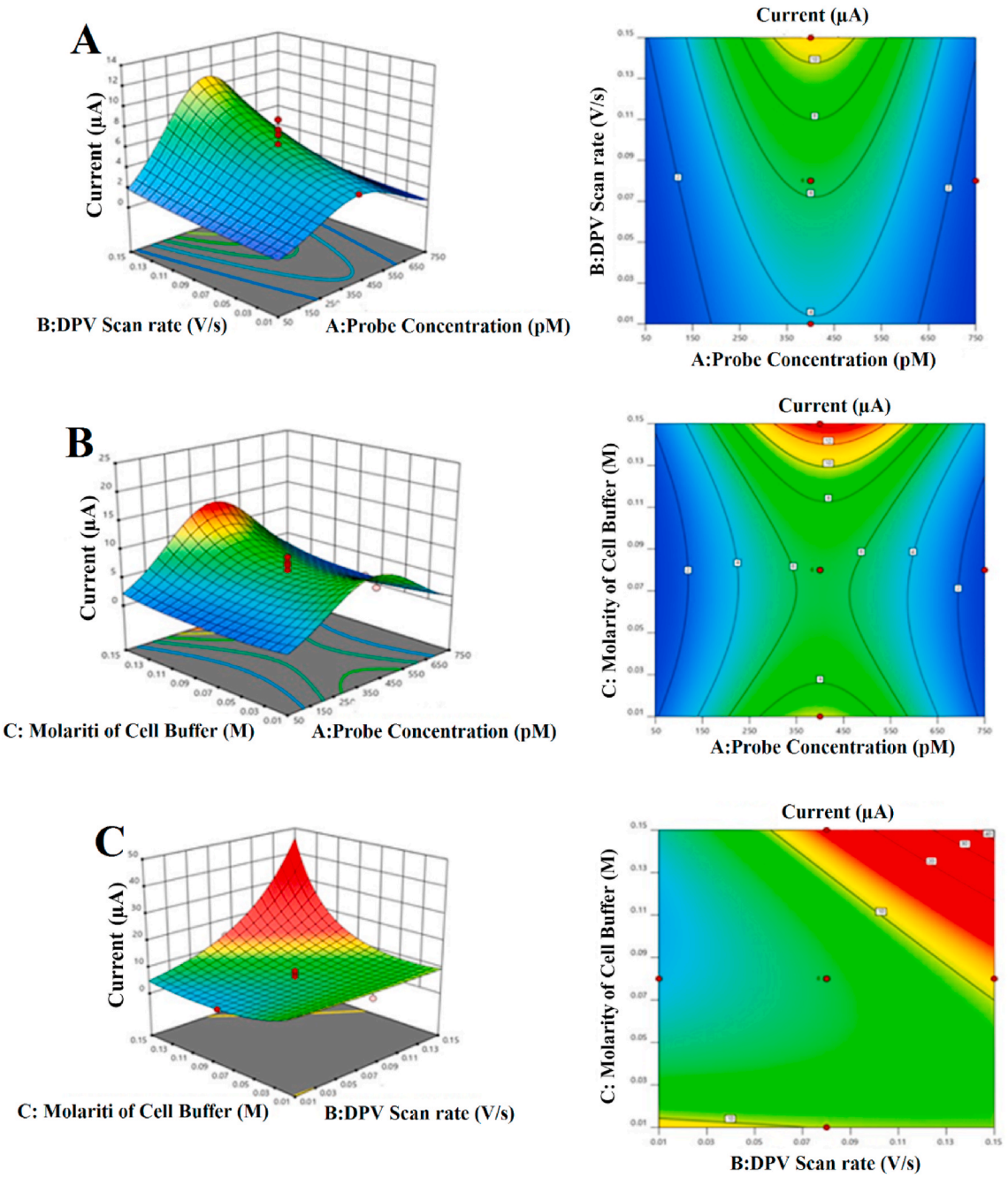

Fig. 2. 3D surface and 2D contour plots of peak current as a function of the combined effect of A) probe concentration-DPV scan rate (A*B), B) molarity of cell buffer-probe concentration (A*C), and C) molarity of cell buffer-DPV scan rate (B*C).

high-burden of bacteria the biosensor detection efficacy will be reduced. About *M. tb* detection, two issues are notable in sensory detection include the low detection limit and an extended range of linear working range. Given that a biosensor can be used for following antibiotic therapy in TB patients. So, if it has been a narrow linear range, it cannot have discriminatory power in differentiating sputum samples with various *M. tb* loads. By contrast, our constructed DNA has a wider detection linear range as well as it is simple and cheap.

The reproducibility of the established biosensor was studied utilizing a set of three independent electrodes to detect the same concentration of target DNA (0.5 nM), resulting in a relative standard deviation of 6.46%, confirming the acceptable reproducibility.

We were examined this test by the whole genome H37Rv *M.tb* strain that has 15–16 copy numbers of the target sequence. Contrary to our expectations based on the increase in the strength of MB oxidation peak by examining the ss-DNA of bacterium whole genome with multiple of the target sequences, the results have exhibited a reduction at methylene blue oxidation peak current. An interpretation for the obtained results was that by increasing the single-strand DNA target length, the misconfiguration and non-specific direction it's on the surface of the electrode has occurred, so the number of the hybrid structures and the peak of MB oxidation were decreased [66,67]. Also, the DNA structure and mode of DNA immobilization and orientation at electrode can influence the MB-DNA interactions and the resulting electrochemical oxidation peak. The usage of the long ss-DNA of bacterium whole genome, avoid from multiple surface contacts between the ss-DNA probe on the electrode surface and ss-DNA target.

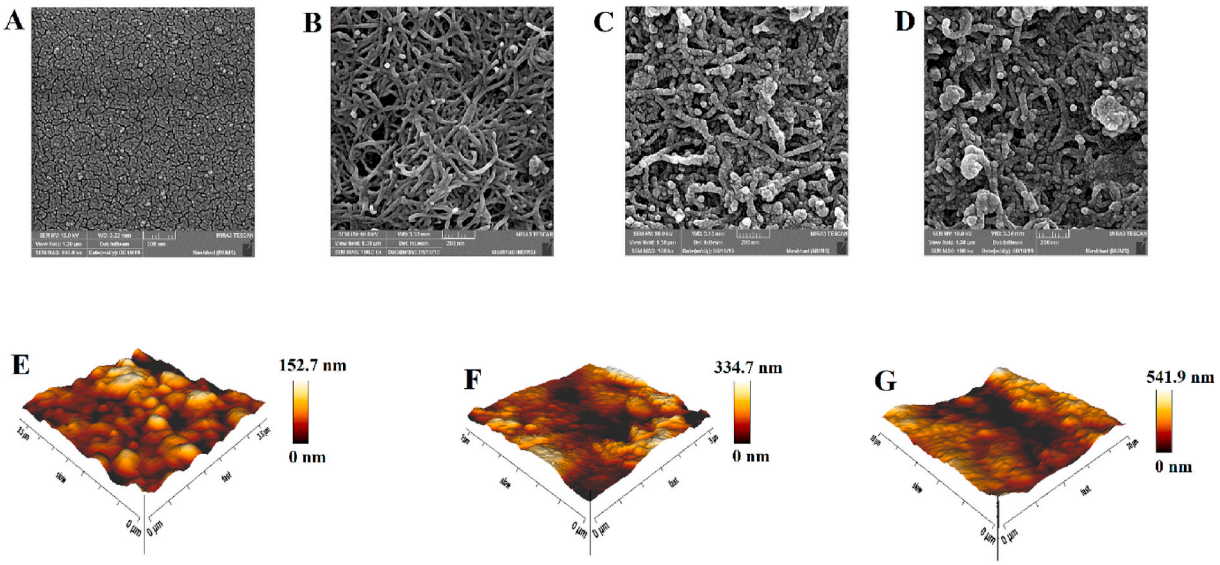

Fig. 3. FE-SEM images of (A) bare GCE, (B) MWCNTs/GCE, (C) PPY/MWCNTs/GCE, (D) HAPNPs/PPY/MWCNTs/GCE. AFM images of (E) HAPNPs/PPY/MWCNTs/GCE, (F) ssDNA/HAPNPs/PPY/MWCNTs/GCE, and (G) dsDNA/HAPNPs/PPY/MWCNTs/GCE.

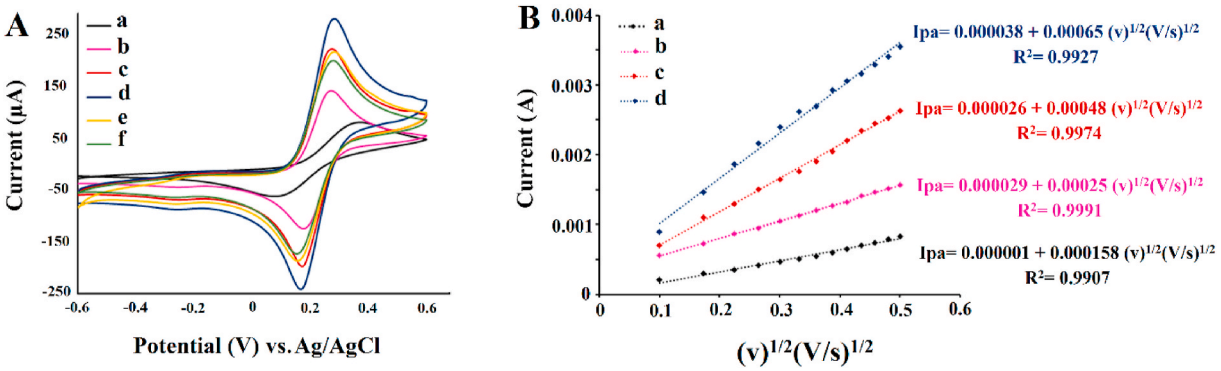

Fig. 4. CVs of different modified electrodes in 1.0 mM $[Fe(CN)_6]^{3-/4-}$ containing 0.1 M KCl, **(a)** bare GCE, **(b)** MWCNTs/GCE, **(c)** PPY/MWCNTs/GCE, **(d)** HAPNPs/PPY/MWCNTs/GCE, **(e)** ssDNA/HAPNPs/PPY/MWCNTs/GCE, and **(f)** dsDNA/HAPNPs/PPY/MWCNTs/GCE, **(B)** Linear curves of **(a)** bare GCE, **(b)** MWCNTs/GCE, **(c)** PPY/MWCNTs/GCE, and **(d)** HAPNPs/PPY/MWCNTs/GCE in 1.0 mM $[Fe(CN)_6]^{3-/4-}$ containing 0.1 M KCl at different scan rates (0.01–0.15 V/s).

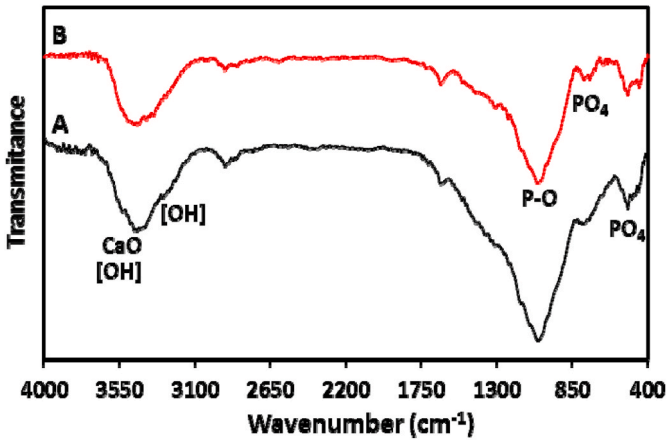

Fig. 5. Spectra FTIR obtained from the HAPNPs/PPY/MWCNTs/GCE **(A)** and ss-DNA/HAPNPs/PPY/MWCNTs/GCE **(B).**

3.4. The specificity detection of the DNA biosensor

We evaluated the DPV response characteristics of the developed biosensor with 100 nM of complementary target, two-bases mismatch target (2mDNA), five-bases mismatch target (5mDNA), and non-complementary sequence (ncDNA) by using ssDNA as capture probe. Fig. 6C shows that the peak current intensity decreased with an increasing number of mismatch base pairs. These results clearly demonstrated that the ssDNA/HAPNPs/PPY/MWCNTs/GCE possessed high specificity for *M. tb* detection.

In order to further study the selectivity of the fabricated biosensor, DPV response generated from two interfering mycobacterial species including *M. simiae* strain TMC 1226 and *M. bovis* BCG strain GL2 were compared. The DPV measurement data in Fig. 6D indicate that designed biosensor is highly specific to only *M. tb* and no significant DPV response is observed for these strains.

3.5. Detection of M.tb in sputum samples

The clinical applicability of the proposed biosensor was studied by measuring its response in the extracted DNA from patient sputum samples which collected from the pathological laboratory in Mashhad. For this purpose, collected human sputum samples (2 tuberculosis-

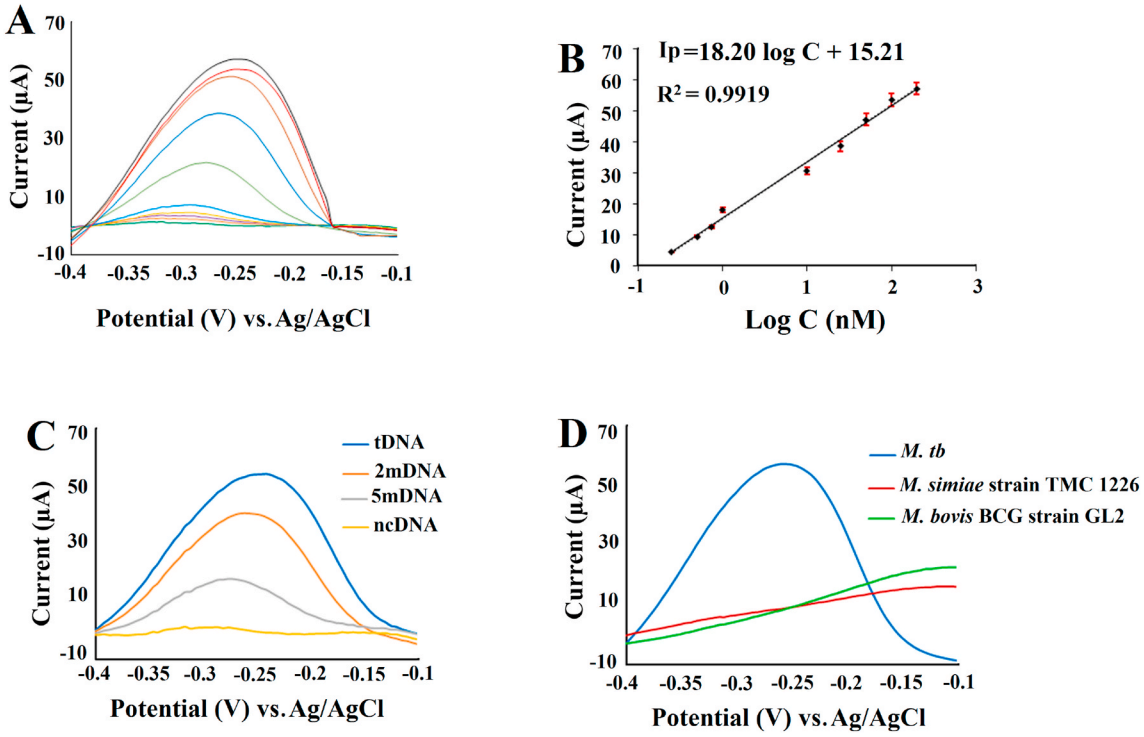

Fig. 6. (A) DPV responses of the biosensor in the presence of different target DNA concentration (0.25, 0.5, 0.75, 1.0, 10.0, 25.0, 50.0, 100.0, 200.0 nM). **(B)** Corresponding calibration plot of the MB oxidation current intensity versus the logarithm of target concentration. (Error bars, SD; n = 3). **(C)** Selectivity of the biosensor in the presence of 2mDNA, 5mDNA, and ncDNA. The concentration of each compound was 100.0 nM. **(D)** Selectivity of the biosensor toward *M.tb* in the presence of *M. simiae* strain TMC 1226 and *M. bovis* BCG strain GL2.

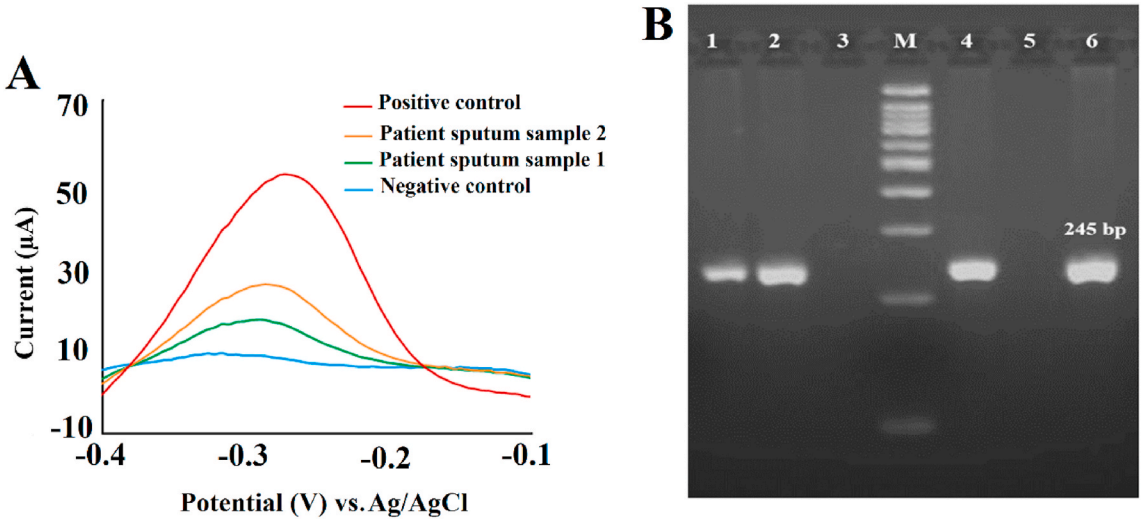

Fig. 7. (A) DPV responses of the biosensor after hybridization with DNA extracted from sputum clinical samples. **(B)** PCR amplification of IS 6110 fragment gene. Lane M: 100 bp DNA marker. Lanes 1 and 2: human sputum DNA samples positive for *M. tb* IS6110 sequence. Lane 3: human sputum DNA sample negative for *M. tb* IS6110 sequence. Lane 4: positive clinical isolate for *M. tb* IS6110 gene sequence from bacterial colony grown on Löwenstein–Jensen medium, lanes 5 & 6: negative and positive (H37 Rv *M. tb* strain) controls for PCR reaction, respectively.

infected and 1 healthy people) was subjected to digestion-contamination process and the boiling method was used for extraction of DNA [68]. Finally, total genome of *M. tb* H37Rv was extracted based Van-Soolingen method [69]. The DPV measurements were performed in these samples using ssDNA/HAPNPs/PPY/MWCNTs/GCE. As displayed in Fig. 7A, the peak current increased significantly in the presence of extracted DNA from positive samples, confirming the occurrence of hybridization in the offered system while incubation with the extracted DNA from the negative sample, resulting in a negligible change in peak current. In fact, by increasing the considered bacterial *M. tb* in the clinical sputum samples, the amount of target DNA can be raised and followed the signal hybridization will be intense. These results were further validated with gel electrophoresis (Fig. 7B). In detail, lane 1 that showing the human sputum DNA sample positive for *M. tb* IS6110 sequence has a narrow DNA gel electrophoresis band but in lane 2, by a remarkable DNA electrophoresis band, the strength of signal hybridization has been higher.

Additionally, the recovery experiment was also carried out in PBS

Table 6
Results for the detection of spiked M.tb in human sputum samples.

Sputum samples	*M. tb* H37Rv Added (nM)	Found (nM)	Recovery (%)	RSD (%)
1	0	Not found	-	-
2	0.100	0.091	91.0	4.21
3	1.00	0.973	97.3	3.10
4	10.0	9.47	94.7	2.50
5	100.0	100.8	100.8	2.032

buffer using 20-fold diluted sputum sample. For recovery studies, we used the human healthy sputum sample that both PCR and sputum culture of M. tb for it were negative. Different concentrations of whole genome of *M. tb* H37Rv were spiked into the diluted sputum sample, and were then analyzed by proposed biosensor. Despite the complex fluid composition, M. tb was successfully detected with good accuracy (recovery%, 91.0–100.08) and high precision (RSD%, 2.03–4.21) (Table 6). Therefore, this biosensor has potential applications for reliable detection of *M. tb* in real clinical samples.

4. Conclusion

The present study describes the fabrication of a PCR-free electrochemical biosensor for reliable detection of *M. tb* using the increased response signals of MB amplified by HAPNPs/PPY/MWCNTs nanocomposite. Optimization studies for probe immobilization parameters and the target hybridization event were conducted using RSM methodology to achieve desirable analysis performances in terms of minimum analysis time and great sensitivity and selectivity. The developed biosensing platform was simple to design and showed excellent specificity for the detection of whole genome of *M. tb* H37Rv in the real sputum samples. This biosensor can serve as a promising screening tool for point–of–care *M. tb* identification in a vulnerable population.

CRediT author contribution statement

Kobra Salimiyan Rizi: Investigation, Data curation, Writing original draft. Behnaz Hatamluyi: Investigation, Re-sources, Writing original draft, review & editing. Majid Rezayi: Conceptualization, Supervision, Methodology, Resources, Investigation, Re-sources, Writing original draft, review & editing. Zahra Meshkat: Conceptualization, Re-sources. Mojtaba Sankian: Methodology, review & editing. Kiarash Ghazvini: review & editing. Hadi Farsiani: review & editing. Ehsan Aryan: Conceptualization, Supervision, Methodology, Resources, Investigation.

Declaration of competing interest

The authors declare that they have no known competing financial interests or personal relationships that could have appeared to influence the work reported in this paper.

Acknowledgements

The authors gratefully acknowledge the University of Medical Sciences Mashhad, Iran for the financial support of current research work.

Appendix A. Supplementary data

Supplementary data to this article can be found online at https://doi.org/10.1016/j.talanta.2021.122099.

References

[1] G. Delogu, M. Sali, G. Fadda, The biology of mycobacterium tuberculosis infection, Mediterranean journal of hematology and infectious diseases 5 (1) (2013).
[2] M. Sypabekova, P. Jolly, P. Estrela, D. Kanayeva, Electrochemical aptasensor using optimized surface chemistry for the detection of Mycobacterium tuberculosis secreted protein MPT64 in human serum, Biosens. Bioelectron. 123 (2019) 141–151.
[3] S. Bizid, S. Blili, R. Mlika, A. Haj Said, H. Korri-Youssoufi, Direct E-DNA sensor of Mycobacterium tuberculosis mutant strain based on new nanocomposite transducer (Fc-ac-OMPA/MWCNTs), Talanta 184 (2018) 475–483.
[4] I. Smith, Mycobacterium tuberculosis pathogenesis and molecular determinants of virulence, Clin. Microbiol. Rev. 16 (3) (2003) 463–496.
[5] P. Sinha, A. Gupta, P. Prakash, S. Anupurba, R. Tripathi, G. Srivastava, Differentiation of Mycobacterium tuberculosis complex from non-tubercular mycobacteria by nested multiplex PCR targeting IS6110, MTP40 and 32kD alpha antigen encoding gene fragments, BMC Infect. Dis. 16 (1) (2016) 123.
[6] S.K. Srivastava, C.J. Van Rijn, M.A. Jongsma, Biosensor-based detection of tuberculosis, RSC Adv. 6 (22) (2016) 17759–17771.
[7] Y. Ko, C. Kim, B. Chang, S.Y. Lee, S.Y. Park, E.K. Mo, S.J. Hong, M.G. Lee, I. G. Hyun, Y.B. Park, Loculated tuberculous pleural effusion: easily identifiable and clinically useful predictor of positive mycobacterial culture from pleural fluid, Tuberc. Respir. Dis. 80 (1) (2017) 35–44.
[8] T.M.S. Alnour, Smear microscopy as a diagnostic tool of tuberculosis: review of smear negative cases, frequency, risk factors, and prevention criteria, Indian J. Tubercul. 65 (3) (2018) 190–194.
[9] J.C. Lin, T.Y. Lin, W.C. Perng, C.S. Mai, Y.H. Chen, C.H. Ku, F.Y. Chang, An outbreak of tuberculosis in a bacillus Calmette-guérin-vaccinated military population, Mil. Med. 173 (4) (2008) 388–392.
[10] M.H. Mat Zaid, J. Abdullah, N.A. Yusof, Y. Sulaiman, H. Wasoh, M.F. Md Noh, R. Issa, PNA biosensor based on reduced graphene oxide/water soluble quantum dots for the detection of Mycobacterium tuberculosis, Sensor. Actuator. B Chem. 241 (2017) 1024–1034.
[11] J. Zhang, Y. Li, S. Duan, F. He, Highly electrically conductive two-dimensional Ti3C2 Mxenes-based 16S rDNA electrochemical sensor for detecting Mycobacterium tuberculosis, Anal. Chim. Acta 1123 (2020) 9–17.
[12] B. Hatamluyi, Z. Es'haghi, Quantitative biodetection of anticancer drug rituxan with DNA biosensor modified PAMAM dendrimer/reduced graphene oxide nanocomposite, Electroanalysis 30 (8) (2018) 1659–1668.
[13] C. Liu, D. Jiang, G. Xiang, L. Liu, F. Liu, X. Pu, An electrochemical DNA biosensor for the detection of Mycobacterium tuberculosis, based on signal amplification of graphene and a gold nanoparticle–polyaniline nanocomposite, Analyst 139 (21) (2014) 5460–5465.
[14] H. Ilkhani, H. Zhang, A. Zhou, A novel three-dimensional microTAS chip for ultra-selective single base mismatched Cryptosporidium DNA biosensor, Sensor. Actuator. B Chem. 282 (2019) 675–683.
[15] H. Thakur, N. Kaur, D. Sareen, N. Prabhakar, Electrochemical determination of M. tuberculosis antigen based on Poly(3,4-ethylenedioxythiophene) and functionalized carbon nanotubes hybrid platform, Talanta 171 (2017) 115–123.
[16] B. Hatamluyi, Z. Es'haghi, Electrochemical biosensing platform based on molecularly imprinted polymer reinforced by ZnO–graphene capped quantum dots for 6-mercaptopurine detection, Electrochim. Acta 283 (2018) 1170–1177.
[17] F.M. Zahed, B. Hatamluyi, F. Lorestani, Z. Es'haghi, Silver nanoparticles decorated polyaniline nanocomposite based electrochemical sensor for the determination of anticancer drug 5-fluorouracil, J. Pharmaceut. Biomed. Anal. 161 (2018) 12–19.
[18] S. Zhao, Y. Zhou, L. Wei, L. Chen, Low fouling strategy of electrochemical biosensor based on chondroitin sulfate functionalized gold magnetic particle for voltammetric determination of mycoplasma ovipneumonia in whole serum, Anal. Chim. Acta 1126 (2020) 91–99.
[19] G. Maduraiveeran, M. Sasidharan, V. Ganesan, Electrochemical sensor and biosensor platforms based on advanced nanomaterials for biological and biomedical applications, Biosens. Bioelectron. 103 (2018) 113–129.
[20] M. Kim, J. Jang, C. Cha, Carbon nanomaterials as versatile platforms for theranostic applications, Drug Discov. Today 22 (9) (2017) 1430–1437.
[21] A. Miodek, N. Mejri-Omrani, R. Khoder, H. Korri-Youssoufi, Electrochemical functionalization of polypyrrole through amine oxidation of poly(amidoamine) dendrimers: application to DNA biosensor, Talanta 154 (2016) 446–454.
[22] E.B. Aydın, M. Aydın, M.K. Sezgintürk, A novel electrochemical immunosensor based on acetylene black/epoxy-substituted-polypyrrole polymer composite for the highly sensitive and selective detection of interleukin 6, Talanta 222 (2021) 121596.
[23] M. Heydari, A. Gholoobi, G. Ranjbar, N. Rahbar, S.B.T. Sany, M.G. Mobarhan, G. A. Ferns, M. Rezayi, Aptamers as potential recognition elements for detection of vitamins and minerals: a systematic and critical review, Crit. Rev. Clin. Lab Sci. 57 (2) (2020) 126–144.
[24] Z. Yang, C. Zhang, Molecularly imprinted hydroxyapatite thin film for bilirubin recognition, Biosens. Bioelectron. 29 (1) (2011) 167–171.
[25] R. Mirzajani, S. Karimi, Preparation of γ-Fe2O3/hydroxyapatite/Cu(II) magnetic nanocomposite and its application for electrochemical detection of metformin in urine and pharmaceutical samples, Sensor. Actuator. B Chem. 270 (2018) 405–416.
[26] S.N. Vakili, M. Rezayi, M. Chahkandi, Z. Meshkat, M. Fani, A. Moattari, A novel electrochemical DNA biosensor based on hydroxyapatite nanoparticles to detect BK polyomavirus in the urine samples of transplant patients, IEEE Sensor. J. 20 (20) (2020) 12088–12095, https://doi.org/10.1109/JSEN.2020.2982948.
[27] B. Derkus, Y.E. Arslan, K.C. Emregul, E. Emregul, Enhancement of aptamer immobilization using egg shell-derived nano-sized spherical hydroxyapatite for thrombin detection in neuroclinic, Talanta 158 (2016) 100–109.

[28] S. Salman, S. Soundararajan, G. Safina, I. Satoh, B. Danielsson, Hydroxyapatite as a novel reversible in situ adsorption matrix for enzyme thermistor-based FIA, Talanta 77 (2) (2008) 490–493.
[29] F. Nemati, M. Hosseini, R. Zare-Dorabei, F. Salehnia, M.R. Ganjali, Fluorescent turn on sensing of Caffeine in food sample based on sulfur-doped carbon quantum dots and optimization of process parameters through response surface methodology, Sensor. Actuator. B Chem. 273 (2018) 25–34.
[30] K.A. Abou-Taleb, G.F. Galal, A comparative study between one-factor-at-a-time and minimum runs resolution-IV methods for enhancing the production of polysaccharide by Stenotrophomonas daejeonensis and Pseudomonas geniculate, Ann. Agric. Sci. 63 (2) (2018) 173–180.
[31] S.N. Vakili, M. Rezayi, M. Chahkandi, Z. Meshkat, M. Fani, A. Moattari, A novel electrochemical DNA biosensor based on hydroxyapatite nanoparticles to detect BK polyomavirus in the urine samples of transplant patients, IEEE Sensor. J. (2020), 1-1.
[32] T.A. Hall, BioEdit: a User-Friendly Biological Sequence Alignment Editor and Analysis Program for Windows 95/98/NT, Nucleic Acids Symposium Series, Information Retrieval Ltd., [London], 1999, pp. 95–98, c1979-c2000.
[33] S. Sankar, S. Kuppanan, B. Balakrishnan, B. Nandagopal, Analysis of sequence diversity among IS6110 sequence of Mycobacterium tuberculosis: possible implications for PCR based detection, Bioinformation 6 (7) (2011) 283.
[34] S. Barreda-García, M.J. González-Álvarez, N. de-los-Santos-Álvarez, J.J. Palacios-Gutiérrez, A.J. Miranda-Ordieres, M.J. Lobo-Castañón, Attomolar quantitation of Mycobacterium tuberculosis by asymmetric helicase-dependent isothermal DNA-amplification and electrochemical detection, Biosens. Bioelectron. 68 (2015) 122–128.
[35] J.S. Stefano, D.P. Rocha, R.M. Dornellas, L.C.D. Narciso, S.R. Krzyzaniak, P. A. Mello, E. Nossol, E.M. Richter, R.A.A. Munoz, Highly sensitive amperometric detection of drugs and antioxidants on non-functionalized multi-walled carbon nanotubes: effect of metallic impurities? Electrochim. Acta 240 (2017) 80–89.
[36] A. Erdem, G. Congur, Hydroxyapatite nanoparticles modified graphite electrodes for electrochemical DNA detection, Electroanalysis 30 (1) (2018) 67–74.
[37] A. Rudnev, N. Vanifatova, T. Dzherayan, A. Burmistrov, Characterization of calcium hydroxyapatite polycrystalline nanoparticles by capillary zone electrophoresis and scanning electron microscopy, J. Anal. Chem. 67 (6) (2012) 565–571.
[38] A. Nassi, F.X. Guillon, A. Amar, B. Hainque, S. Amriche, D. Maugé, E. Markova, C. Tsé, P. Bigey, M. Lazerges, F. Bedioui, Electrochemical DNA-biosensors based on long-range electron transfer: optimization of the amperometric detection in the femtomolar range using two-electrode setup and ultramicroelectrode, Electrochim. Acta 209 (2016) 269–277.
[39] K.-J. Huang, Y.-J. Liu, H.-B. Wang, Y.-Y. Wang, A sensitive electrochemical DNA biosensor based on silver nanoparticles-polydopamine@graphene composite, Electrochim. Acta 118 (2014) 130–137.
[40] H. Li, S. van den Driesche, F. Bunge, B. Yang, M.J. Vellekoop, Optimization of on-chip bacterial culture conditions using the Box-Behnken design response surface methodology for faster drug susceptibility screening, Talanta 194 (2019) 627–633.
[41] R.V. Lenth, Quick and easy analysis of unreplicated factorials, Technometrics 31 (4) (1989) 469–473.
[42] M.H. Pournaghi-Azar, M.S. Hejazi, E. Alipour, Developing an electrochemical deoxyribonucleic acid (DNA) biosensor on the basis of human interleukine-2 gene using an electroactive label, Anal. Chim. Acta 570 (2) (2006) 144–150.
[43] T. Doneux, A. De Rache, E. Triffaux, A. Meunier, M. Steichen, C. Buess-Herman, Optimization of the probe coverage in DNA biosensors by a one-step coadsorption procedure, ChemElectroChem 1 (1) (2014) 147–157.
[44] S.O. Kelley, J.K. Barton, N.M. Jackson, M.G. Hill, Electrochemistry of methylene blue bound to a DNA-modified electrode, Bioconjugate Chem. 8 (1) (1997) 31–37.
[45] S.D. Keighley, P. Li, P. Estrela, P. Migliorato, Optimization of DNA immobilization on gold electrodes for label-free detection by electrochemical impedance spectroscopy, Biosens. Bioelectron. 23 (8) (2008) 1291–1297.
[46] H. Zhou, Nucleic Acid Amplification Strategies for Biosensing, Bioimaging, and Biomedicine, Nucleic Acid Amplification Strategies for Biosensing, Bioimaging and Biomedicine, Springer2019, pp. 3-14.
[47] Z. Izadi, M. Sheikh-Zeinoddin, A.A. Ensafi, S. Soleimanian-Zad, Fabrication of an electrochemical DNA-based biosensor for Bacillus cereus detection in milk and infant formula, Biosens. Bioelectron. 80 (2016) 582–589.
[48] D.A. Oliveira, J.V. Silva, J.M.R. Flauzino, A.C.H. Castro, A.C.R. Moço, M.M.C. N. Soares, J.M. Madurro, A.G. Brito-Madurro, Application of nanomaterials for the electrical and optical detection of the hepatitis B virus, Anal. Biochem. 549 (2018) 157–163.
[49] A.F.-J. Jou, Y.-J. Chen, Y. Li, Y.-F. Chang, J.-j. Lee, A.T. Liao, J.-a.A. Ho, Target-triggered, dual amplification strategy for sensitive electrochemical detection of a lymphoma-associated MicroRNA, Electrochim. Acta 236 (2017) 190–197.
[50] B. Hatamluyi, M. Rezayi, H.R. Beheshti, M.T. Boroushaki, Ultra-sensitive molecularly imprinted electrochemical sensor for patulin detection based on a novel assembling strategy using Au@Cu-MOF/N-GQDs, Sensor. Actuator. B Chem. 318 (2020) 128219.
[51] B. Hatamluyi, Z. Es'haghi, A layer-by-layer sensing architecture based on dendrimer and ionic liquid supported reduced graphene oxide for simultaneous hollow-fiber solid phase microextraction and electrochemical determination of anti-cancer drug imatinib in biological samples, J. Electroanal. Chem. 801 (2017) 439–449.
[52] L. Berzina-Cimdina, N. Borodajenko, Research of calcium phosphates using Fourier transform infrared spectroscopy, Infrared Spectroscopy-Materials Science, Engineering and Technology 12 (7) (2012) 251–263.
[53] P. Raizada, P. Shandilya, P. Singh, P. Thakur, Solar light-facilitated oxytetracycline removal from the aqueous phase utilizing a H2O2/ZnWO4/CaO catalytic system, Journal of Taibah University for Science 11 (5) (2017) 689–699.
[54] A. Destainville, E. Champion, D. Bernache-Assollant, E. Laborde, Synthesis, characterization and thermal behavior of apatitic tricalcium phosphate, Mater. Chem. Phys. 80 (1) (2003) 269–277.
[55] S.J. Gutiérrez-Prieto, L.F. Fonseca, L.G. Sequeda-Castañeda, K.J. Díaz, L. Y. Castañeda, J.A. Leyva-Rojas, J.C. Salcedo-Reyes, A.P. Acosta, Elaboration and biocompatibility of an eggshell-derived hydroxyapatite material modified with Si/PLGA for bone regeneration in dentistry, International journal of dentistry (2019) 2019.
[56] K. Salma, N. Borodajenko, A. Plata, L. Berzina-Cimdina, A. Stunda, Fourier Transform Infrared Spectra of Technologically Modified Calcium Phosphates, 14th Nordic-Baltic Conference on Biomedical Engineering and Medical Physics, Springer, 2008, pp. 68–71.
[57] P. Thawornpan, S. Thanapongpichat, A.W. Tun, W. Jumpathong, L.d. Jong, H. Buncherd, Isolation of nucleic acids using fly ash as a low-cost adsorbent, Anal. Lett. (2020) 1–14.
[58] Z. Yan-Zhong, H. Yan-Yan, Z. Jun, Z. Shai-Hong, L. Zhi-You, Z. Ke-Chao, Characteristics of functionalized nano-hydroxyapatite and internalization by human epithelial cell, Nanoscale research letters 6 (1) (2011) 1–8.
[59] P. Mahmoodi, M. Rezayi, E. Rasouli, A. Avan, M. Gholami, M. Ghayour Mobarhan, E. Karimi, Y. Alias, Early-stage cervical cancer diagnosis based on an ultra-sensitive electrochemical DNA nanobiosensor for HPV-18 detection in real samples, J. Nanobiotechnol. 18 (1) (2020) 11.
[60] M. Rezayi, R. Karazhian, Y. Abdollahi, L. Narimani, S.B.T. Sany, S. Ahmadzadeh, Y. Alias, Titanium (III) cation selective electrode based on synthesized tris (2pyridyl) methylamine ionophore and its application in water samples, Sci. Rep. 4 (2014) 4664.
[61] S. Mariani, S. Scarano, J. Spadavecchia, M. Minunni, A reusable optical biosensor for the ultrasensitive and selective detection of unamplified human genomic DNA with gold nanostars, Biosens. Bioelectron. 74 (2015) 981–988.
[62] M.M. Rahman, M.M. Hussain, A.M. Asiri, A novel approach towards hydrazine sensor development using SrO· CNT nanocomposites, RSC Adv. 6 (70) (2016) 65338–65348.
[63] M. Fani, M. Rezayi, H.R. Pourianfar, Z. Meshkat, M. Makvandi, M. Gholami, S. A. Rezaee, Rapid and label-free electrochemical DNA biosensor based on a facile one-step electrochemical synthesis of rGO–PPy–(l-Cys)–AuNPs nanocomposite for the HTLV-1 oligonucleotide detection, Biotechnol. Appl. Biochem. (2020).
[64] A. Miodek, N. Mejri, M. Gomgnimbou, C. Sola, H. Korri-Youssoufi, E-DNA sensor of Mycobacterium tuberculosis based on electrochemical assembly of nanomaterials (MWCNTs/PPy/PAMAM), Anal. Chem. 87 (18) (2015) 9257–9264.
[65] Z. Hatami, E. Ragheb, F. Jalali, M.A. Tabrizi, M. Shamsipur, Zinc oxide-gold nanocomposite as a proper platform for label-free DNA biosensor, Bioelectrochemistry 133 (2020) 107458.
[66] E. Farjami, L. Clima, K.V. Gothelf, E.E. Ferapontova, DNA interactions with a methylene blue redox indicator depend on the DNA length and are sequence specific, Analyst 135 (6) (2010) 1443–1448.
[67] P. Mahmoodi, M. Rezayi, E. Rasouli, A. Avan, M. Gholami, M.G. Mobarhan, E. Karimi, Y. Alias, Early-stage cervical cancer diagnosis based on an ultra-sensitive electrochemical DNA nanobiosensor for HPV-18 detection in real samples, J. Nanobiotechnol. 18 (1) (2020) 1–12.
[68] S.I. Cadmus, O.I. Falodun, O.E. Fagade, Methods of sputum decontamination with emphasis on local tuberculosis laboratories, Afr. J. Med. Med. Sci. 40 (1) (2011) 5–14.
[69] D. Van Soolingen, P. De Haas, P. Hermans, P. Groenen, J. Van Embden, Comparison of various repetitive DNA elements as genetic markers for strain differentiation and epidemiology of Mycobacterium tuberculosis, J. Clin. Microbiol. 31 (8) (1993) 1987–1995.